乱流の Large-eddy simulation の最近の話題(計算流体力学に関わる数理的諸問題)

AUTHOR(S):

堀内, 潔

CITATION:

堀内, 潔. 乱流の Large-eddy simulation の最近の話題(計算流体力学に関わる数理的諸問題). 数理解析研究所講究録 1996, 974: 122-127

ISSUE DATE:

1996-11

URL:

http://hdl.handle.net/2433/60763

数理解析研究所講究録
974巻 1996年 122-127

乱流の Large-eddy simulation の最近の話題

東京工業大学工学部機械宇宙学科　堀内　潔

Direct numerical simulation (DNS) data have been used in order to analyze the energy transfer between the grid scale (GS) and subgrid-scale (SGS) in large eddy simulations (LES) of the wall bounded and free shear turbulent flows. Previously, a significant occurrence of backward (B-) cascade of SGS energy has been reported. In the present study, this B- cascade event is investigated correlating to the coherent structures observed in both flows, using the conditional ensemble averaging technique. It is found that the strong B- cascade is principally generated along the elliptic cross section vortices in which the major axis is tilted against the spanwise axis. In the assessment of the SGS models, a poor performance of the eddy viscosity models in approximating the fine vortical structure generating the B-cascade was found, whereas the scale-similarity models very accurately represented these structures.

1. INTRODUCTION

In the analysis of the energy transfer between grid-scale (GS) and subgrid-scale (SGS) in large eddy simulations (LES) of the wall bounded flow, [1] [2] [3] [4] [5] and in free shear turbulent flow, [5] it was shown that the forward (F-) and (B-) backward cascades of SGS energy were typically of the same order of magnitude, with the net transfer being slightly from GS to SGS. A new SGS models capable of an accurate prediction of B- cascade effect, while properly absorbing GS energy into SGS, was presented in Horiuti. [4] [5]

Coherent structures are known to exist in the wall-bounded and free shear turbulent flows such as the streaks in the former and the rib vortices in the latter. The aim of the present study is to investigate the SGS energy generation mechanism in relation to the coherent vortical structures in both flows, and make assessment on the SGS model that can accurately approximates the fine-scale structure of these vortices. A particular emphasis will be placed on the B-cascade effect.

The subgrid-scale stress tensor, τ_{ij}, that results from filtering the Navier-Stokes equations consists of three terms: [6] $\tau_{ij} = L_{ij} + C_{ij} + R_{ij}$, where L_{ij} is the Leonard term, C_{ij} is the cross term, and R_{ij} is the SGS Reynolds stress $\overline{u_i'u_j'}$. $\overline{u}_i$ denotes the GS velocity component of u_i and $u_i' = u_i - \overline{u}_i$ denotes the SGS component. The indices $i = 1, 2, 3$ correspond to the directions x, y, and z, respectively, with x being the streamwise, y wall-normal or cross-stream, and z the spanwise directions. The fields we consider in the present study are homogeneous in two-directions. In these directions (x and z), a two-dimensional Gaussian filter was used. In the following, $\langle\rangle$ denotes the average in the $x-z$ plane. In the present study, we deal with only the R_{ij} terms. [6] [7] GS and SGS fields interact through the SGS production term $P = -\overline{u_i'u_j'}(\partial\overline{u}_i/\partial x_j + \partial\overline{u}_j/\partial x_i)/2$. When P is non-negative, the GS energy is forwardly transferred into SGS (F-cascade), while if P is negative the SGS energy is in turn transferred backwardly into the GS (B-cascade). In the present study, we make use of the Direct Numerical Simulation (DNS) flow fields to directly test the GS-SGS energy transfer.

2. DNS DATA ANALYSIS

2.1 Mixing layer

The free shear turbulence that we have chosen is the incompressible mixing layer flow which develops in time. [8] We generated the DNS data

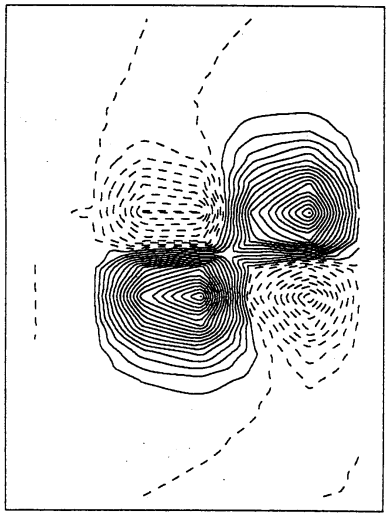

Figure 1: End view of P at $t = 350$ in the $y - z$ plane at $x = 52.5\theta_0$ from mixing layer DNS data (Contour levels from -0.0003 to 0.0005 (with increment of 0.000025)); R_{ij} terms estimated from the exact DNS data, a portion of $y = -3.56\theta_0 \sim 1.67\theta_0$ and $z = 36.9\theta_0 \sim 40.8\theta_0$ is shown.

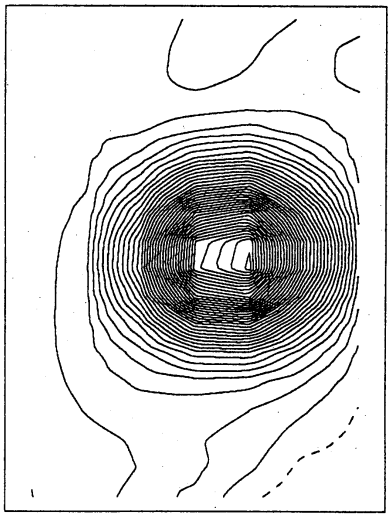

Figure 2: End view of the GS streamwise vorticity $\overline{\omega}_x$ at $t = 350$ in the $y - z$ plane at $x = 52.5\theta_0$ from mixing layer DNS data ($-0.1 \sim 0.4(0.02)$); the same portion as in Fig.1 is shown.

for transitional and turbulent regimes using the Fourier/finite difference method, where 192, 128 and 128 grid points were used respectively in the x, y and z directions. The initial momentum thickness θ_0 was 1, and its vorticity thickness δ_i was $\sqrt{2}\pi$. The size of the computational domain was $14\delta_i$, $56\delta_i$ and $9.3\delta_i$, respectively in the x, y, and z directions. Periodic boundary conditions were employed in the $x - z$ directions, while a free slip boundary condition was imposed in the y direction. The Reynolds number Re_θ based on the mean velocity difference at the both edges of the mixing layer, ΔU, and θ_0 was set equal to 200. The sinusoidal random fluctuations confined to the vorticity thickness region in the y-direction were superposed to the initial mean error function velocity profile. [5] The mixing layer flow field was filtered to $96 \times 129 \times 64$ grid points, respectively in the x, y and z directions.

In the spatial distributions of P which was estimated from the exact DNS terms at $t = 350$, it was found that a large SGS energy production occurs in the braid region of the layer. [9] At this time, the roll-up of the Kelvin-Helmholtz(K-H)vortices was complete, and these two eddies started to merge. The predominantly streamwise vortices ("rib" vortices) resided in the braid region between the K-H rollers. [10] The production term was characterized by a very intermittent appearance of the strong F- and B- cascade regions, that take place side by side with a quadruple-like structure. A typical example is magnified in Fig.1 of the end view of the contours of P. Positive values are plotted by the solid lines, and the negative ones by the dashed lines.

This quadruple structure is highly aligned with the rib vortices. The end view of the contours of the GS streamwise vorticity $\overline{\omega}_x (= \partial\overline{v}/\partial z - \partial\overline{w}/\partial y)$ in the same cross-section as in Fig.1 is shown in Fig.2. This rib vortex was elongated in the downstream direction, with its downstream extent being $\approx 35\theta_0$. F-cascade is generated in the 1st and 3rd quadrants of the rib vortices, and B-cascade in the 2nd and 4th quadrants. We consider that the presence of these rib vortices is the primary cause of the almost equal occurrence of F- and B- cascades in the mixing layer. The present result indicates that the B-cascade may be rather deterministic.

The presented quadruple structure is akin to the example pointed out by Jiménez, [11] in which there was no net transfer of energy, but contained

regions of localized F- and B- cascades. The energy transfer is reversible in his example. On the contrary, in the present example, the vorticity distribution is not completely circular, rather elliptic. The circulation of this elliptic vortex is counter clockwise. This ellipse may be identified because the structure is lying at an angle to the streamwise direction. [12] The rib vortices' inclination angle to the mean shear plane was $\approx$ 28 degrees. We have examined the vorticity contours projected onto the plane perpendicular to the axis of this rib vortex. Its cross section was also elliptic, and its aspect ratio of the minor axis against the major axis was even smaller than in the ellipse shown in Fig.2.

The major axis of this ellipse is lying at a positive angle at the cross-stream (y) axis. As a result, the area of 1st and 3rd quadrants is larger than the 2nd and 4th quadrants. Subsequently, the magnitude of F-cascade was higher than the B-cascade, i.e., the net energy cascade in the plotted region was forward. The total summations of actual F- and B- cascade term values were 0.0046 and -0.0018, respectively. Similarly, clockwise elliptic vortices were found in the DNS data, and their major axis was lying at a negative angle at the y axis, the resultant net-cascade was also forward. In both ellipse, the energy transfer is irreversible.

Similar inclined ellipse has been often found in the roller eddies. A conventional direct explanation for an occurrence of negative production in the roller is that, when the major axis of the ellipse is aligned with the direction of the mean shear, the area in which a positive correlation of the streamwise and normal SGS fluctuations takes place (2nd and 4th quadrants) is larger than the area in which a negative correlation of them takes place (1st and 3rd quadrants). [9]

This is opposite to the SGS production term distribution found here. The reason was that, unlike in the rollers, the shear production term ($P_{23} = -\overline{u_2'u_3'}(\partial\overline{u}_2/\partial x_3 + \partial\overline{u}_3/\partial x_2)$) was not dominant among the SGS production terms in the present rib vortex. Most dominant one was the normal production term of (2,2) component,

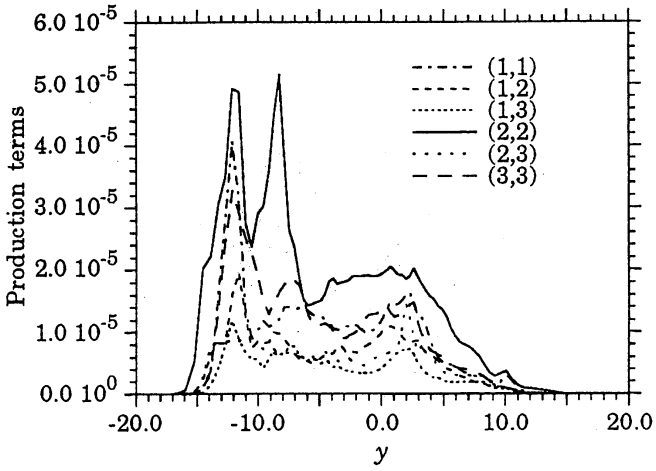

Figure 3: $y-$distribution of rms values of P_{ij} terms from the mixing layer DNS data; R_{ij} terms estimated from the exact DNS data.

i.e., $P_{22} = -\overline{u_2'u_2'}\partial\overline{u}_2/\partial x_2$. Figure 3 shows the $y-$distributions of rms values of each terms $P_{ij} = -\overline{u_i'u_j'}(\partial\overline{u}_i/\partial x_j + \partial\overline{u}_j/\partial x_i)/2$ (no summation in i and j), from the mixing layer. It can be seen that the most dominant terms are the diagonal components of P_{11}, P_{22} and P_{33} terms. Among these terms, P_{22} term distribution was highly correlated with the distribution of P, and a quadruple structure of P in Fig.1 primarily arose in P_{22} term. The shear stress production terms P_{23} and P_{12} contribution is insignificant. In fact, the contours of P_{23} term in the same region showed no correlation with the total production term P in Fig.1.

2.2 Channel

As for the wall-bounded turbulence, we used the fully developed incompressible channel flow DNS data at Re_τ (Reynolds number based on the wall-friction velocity, u_τ, and the half channel height, δ)=180. [13] Fourier - Chebyshev polynomial expansion method was used with 128, 129 and 128 grid points respectively in the x, y and z directions, In the following, y_+ denotes the wall coordinate $u_\tau y/\nu$, ν is the kinematic viscosity. The channel flow field was filtered to $32\times129\times32$.

Figures 4 shows the $y-$distributions of plane-averaged P_{ij} terms from the channel flow. These terms were decomposed into two-parts which con-

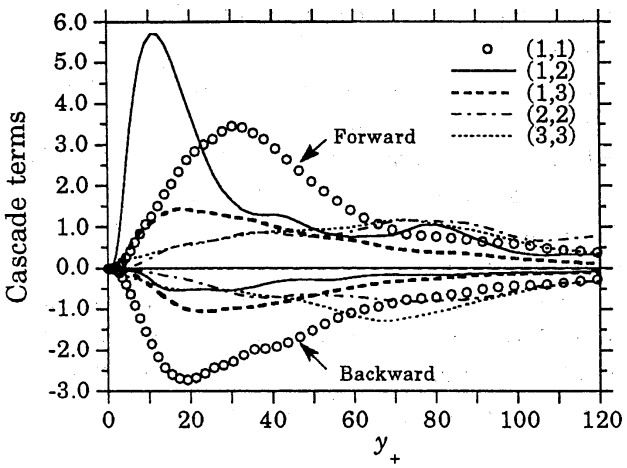

Figure 4: y-profiles of plane averaged F- and B-cascade contributions in P_{ij} terms from channel.

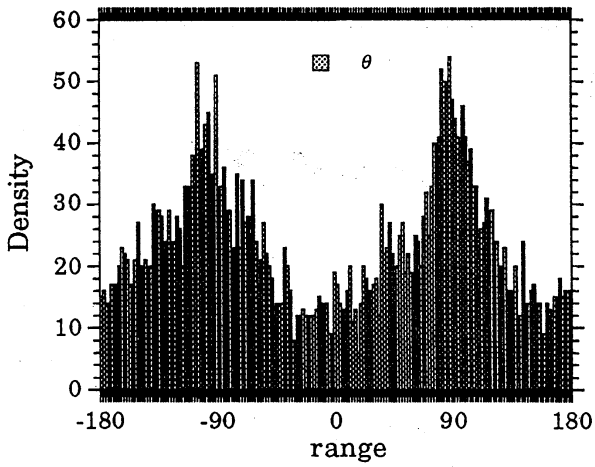

Figure 5: Distribution of the inclination angle θ from the channel flow DNS data at $y_+ = 12$.

tribute to F- ($P_{ij} > 0$) and B- ($P_{ij} < 0$) cascades. It is found that the shear production term, P_{12}, is dominant in the very vicinity of the wall. The cascade arising in this term is predominantly forward due to the presence of the large mean shear rate near the wall. [3] [4] [5] Away from the wall, P_{12} term becomes gradually insignificant, rather, as in the mixing layer, the normal production term, particularly P_{11} term, becomes dominant. Significant B-cascade arises in P_{11} term at $y_+ \approx 15$. It can be seen that the magnitude of F- and B- cascade terms in P_{11} is very close each other, with the total sum of P_{11} being slightly positive.

To detect the dominant vortical structures, the inclination angle to the $x-z$ plane of the projection of the vorticity vector in the $x-y$ planes, $\theta = \tan^{-1}(\overline{\omega}_y/\overline{\omega}_x)$, was calculated at each grid point, where $\overline{\omega}_y$ denotes the GS normal vorticity $\overline{\omega}_y (= \partial\overline{u}/\partial z - \partial\overline{w}/\partial x)$. Figures 5 shows the histograms of θ taken at the $x-z$ plane located at $y_+ = 12$. θ is concentrated around $\pm 90°$, i.e., the dominant structures are placed perpendicular to the wall. Away from the wall at $y_+ \approx 100$, it was concentrated around 45° and 135° in a good accordance with the previous analysis. [14]

In order to further correlate these perpendicular vortices and P_{11} term to the B-cascade, we investigated instantaneous flow fields by applying a conditional averaging procedure. [3] SGS production and velocity fields were averaged for events that corresponded to strong B- cascades. One-point conditions of the type $P_{11} < -3.0\langle P_{11}\rangle$, was imposed at the $x-z$ plane at $y_+ = 12$. Each time an event was detected, the whole GS velocity field was stored, centering on the event. All the realizations where the condition was satisfied were then averaged to yield the conditionally-averaged fields. [15]

The normal vorticity field $\overline{\omega}_y$ was calculated from the velocity field thus obtained. Figure 6 shows the contours of $\overline{\omega}_y$ computed by further imposing the constraint that the circulation is anti-clockwise ($\overline{\omega}_y > 0$). As was found in the mixing layer, the cross-section of the vortex is elliptic, and its major axis is lying at a negative angle at the spanwise (z) axis. When a similar averaging was done for the clockwise normal vorticity ($\overline{\omega}_y < 0$) events, a similar elliptic cross-section vortex was obtained, with its major-axis lying at a positive angle at the z-axis. Subsequently, the net energy cascade along this normal vortex is backward, consistently with the imposed conditional averaging. In both mixing layer and channel flows, the inclined elliptic vortices were the primary generation mechanism of the B-cascade event.

3. SGS MODELS

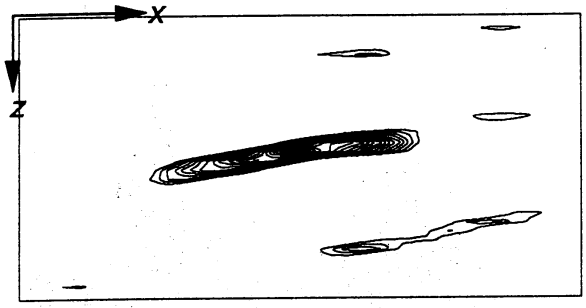

Figure 6: Top view of the conditionally averaged GS normal vorticity $\overline{\omega}_y$ in the $x-z$ plane at $y_+ = 12.0$ from channel flow ($8 \sim 25(1)$)

As for the SGS models, we have conducted assessment on the isotropic eddy viscosity model (EVM) (Smagorinsky [16]), non-isotropic EVM (generalized normal stress (GNS) [13]) and the Bardina model. [6] In the Filtered-Bardina (F-Bardina) model, [4] [5] the Bardina model was modified to incorporate the non-local effect as

$$\overline{u_i' u_j'} = C_B \overline{(\overline{u}_i - \overline{\overline{u}}_i)(\overline{u}_j - \overline{\overline{u}}_j)} \qquad (1)$$

Their performance in representing the quadruple-like structure of SGS production term P (Fig.1) is compared in Figs.7 and 8. A poor performance of the Smagorinsky model is evident; its prediction is symmetric with respect to the spanwise (z) axis unlike the real value, and a large F-cascade is generated even in the region in which a large B-cascade took place in the real value. It is notable that the Smagorinsky model tends to overly estimate the SGS production in the non-turbulent region, indicating an inability of the Smagorinsky model to correctly predict the entrainment of the non-turbulent region by the vortical turbulent region. Its correlation coefficient ($C.C.$) with the real value in the plotted region was very low (0.28). The GNS model prediction was asymmetric with respect to the z axis, with an excessive prediction of F-cascade in the 2nd and 4th quadrants that occurred in the Smagorinsky model being significantly reduced (figure not shown). Its $C.C.$ value was significantly improved to 0.48. The F-Bardina model is very accurate, and $C.C.$ was 0.98. In the Bardina model (figure not shown), it was slightly lower (0.94).

Inaccuracy of the EVM to accurately predict the fine scale structures of the vortices is attributable to a poor representation of vorticity dynamics in the conventional SGS EVM, whereas the scale-similarity models can provide more accurate predictions.

When the EVM is used, the corresponding SGS terms in the governing equations of the vorticity derived by taking the curl of the filtered Navier-Stokes equation approximately becomes

$$\nu_e \frac{\partial^2 \overline{\omega_i}}{\partial x_j \partial x_j}, \qquad (2)$$

where, ν_e is the SGS eddy viscosity coefficient. Thus, in the vorticity equation, R_{ij} terms results in merely a diffusion term of vorticity in the EVM, whereas when the Bardina model is used, R_{ij} terms yields the SGS vorticity stretching terms:

$$C_B(\overline{\omega_j} - \overline{\overline{\omega_j}}) \frac{\partial}{\partial x_j}(\overline{u}_i - \overline{\overline{u}}_i). \qquad (3)$$

Similar terms can be derived when the F-Bardina model [5] is used. Therefore, the SGS vorticity stretching effect is better represented by the scale-similarity models.

4. CONCLUSIONS

The mechanism of energy transfer between the grid scale (GS) and subgrid-scale (SGS) in large eddy simulations (LES), is investigated correlating to the coherent structures in the wall bounded and free shear turbulent flows. It was previously shown that the forward (F-) and backward (B-) cascades of energy transfer arising in both flows are typically of the same order of magnitude, with the net transfer being slightly from GS to SGS. The present direct numerical simulation (DNS) data analysis showed that the strong B- cascade arose in the SGS normal production terms rather than in the shear production terms. In channel, this strong B- cascade event was observed along the vortices perpendicular to the wall. In the mixing layer, the strong F- and B- cascades

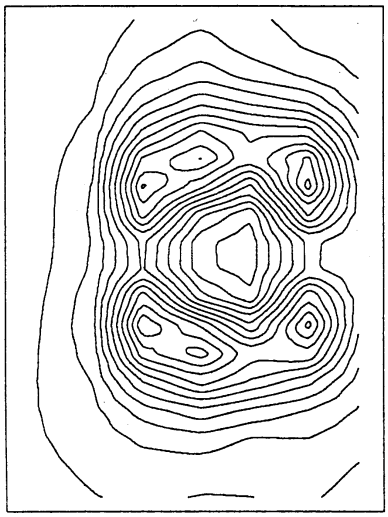

Figure 7: End view of modeled P at $t = 350$ in the $y - z$ plane at $x = 52.5\theta_0$ from mixing layer; the same portion as in Fig.1 is shown, and R_{ij} terms implied by the Smagorinsky model ($0.0 \sim 0.00025(0.00002)$),.

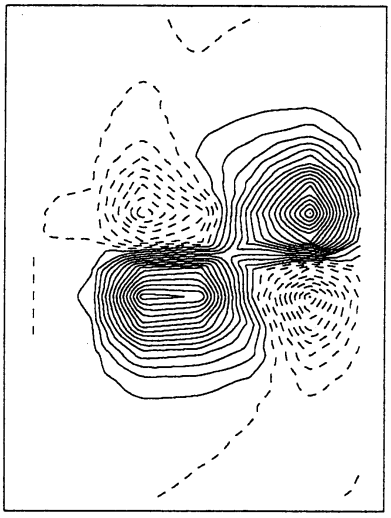

Figure 8: End view of modeled P at $t = 350$. R_{ij} terms implied by the F-Bardina model ($-0.00015 \sim 0.00025(0.0000125)$).

took place side by side along the rib vortices in the braid region. The cross section of these vortices were elliptic in both flows, with their major axis lying tilted against the spanwise axis. As for the subgrid-scale models, assessment is made on the isotropic and non-isotropic eddy viscosity coefficient models and the scale-similarity models. A poor performance of the eddy viscosity models in approximating the fine structure of the SGS production terms was found, whereas the scale-similarity models very accurately represented these structures.

This work was partially supported by the Grant-in-aid, Ministry of Education, Japan (No.05240108)

References

1) U. Piomelli, T.A. Zang, C.G. Speziale, and M.Y. Hussaini, Phys. Fluids A2, 257 (1990).

2) U. Piomelli, W.H. Cabot, P. Moin, and S. Lee, Phys. Fluids A3, 1766 (1991).

3) C. Härtel, L. Kleiser, U. Friedemann, and R. Friedrich, Phys. Fluids , 3130 (1994).

4) K. Horiuti, Proc. of 10th Turbulent Shear Flows Symposium 2, p.20.13-p.20.18 (1995).

5) K. Horiuti, submitted to Phys. Fluids (1995).

6) J. Bardina, Ph.D. dissertation, Stanford University, Stanford, California (1983).

7) K. Horiuti, Phys. Fluids A 1, 426 (1989).

8) N.N. Mansour, Ph.D. dissertation, Stanford University, Stanford, California (1978).

9) A.K.M.F. Hussain, J. Fluid Mech. 173, 303 (1986).

10) M.M. Rogers and R.D. Moser, J. Fluid Mech. 243, 183 (1992).

11) J. Jiménez, Center for Turbulence Research, Annual Reserach Briefs 1993, 171 (1993).

12) P.S. Bernard, J.M. Thomas and R.A. Handler, J. Fluid Mech. 253, 385 (1993).

13) K. Horiuti, Phys. Fluids A 5, 146 (1993).

14) P. Moin and J. Kim, J. Fluid Mech. 155, 441 (1985).

15) U. Piomelli, Y. Yunfang and R.J. Adrian, Submitted to Phys. Fluids (1995).

16) J. Smagorinsky, Mon. Weath. Rev. 91, 99 (1963).